CMS HCal

Summerstudent Program 2009, DESY

Ilka Geisel[a]

[a] Leibniz Universität Hannover

September 9, 2009

Abstract

This report describes the work done in the DESY summer student program at the CMS group related to the hadronic calorimeter (HCal). During this program Monte-Carlo events describing the energy deposition due to particle showers in the HCal were generated. The generated events were used to compare different shower algorithms among each other and with test beam data. Methods for the improvement of the energy resolution and linearity of the calorimeter have been discussed in reference to the planned CMS HCal upgrade.

Contents

1 Introduction **2**

2 Compact Muon Solenoid (CMS) **2**

2.1 Inner tracking system 3

2.2 Electromagnetic calorimeter (ECal) 3

2.3 Hadronic calorimeter (HCal) 3

2.4 Magnet 4

2.5 Muon system 5

3 Simulating Data **6**

3.1 Geant3 program 6

3.2 Shower algorithms 7

3.3 Comparison to test beam results 7

4 Weighting **11**

4.1 Readout schemes and weighting results 11

5 Conclusion **12**

1 Introduction

For approximately 2014 a hardware upgrade of the HCal of the CMS is planned. It will include the longitudinal division of the single towers into 4 readout channels. In the following report the advantages of this upgrade will be shown and different approaches discussed.

- The second chapter gives an overview over the CMS detector. It focuses on the hardware especially on that of the hadronic calorimeter.
- The third chapter shows how the Monte-Carlo events were generated and how the different shower algorithms behave. It also compares the Monte-Carlo events with real data.
- In the fourth chapter the weighting of the events and the advantages of this procedure are shown.
- The fifth chapter concludes this report and gives an outlook.

2 Compact Muon Solenoid (CMS)

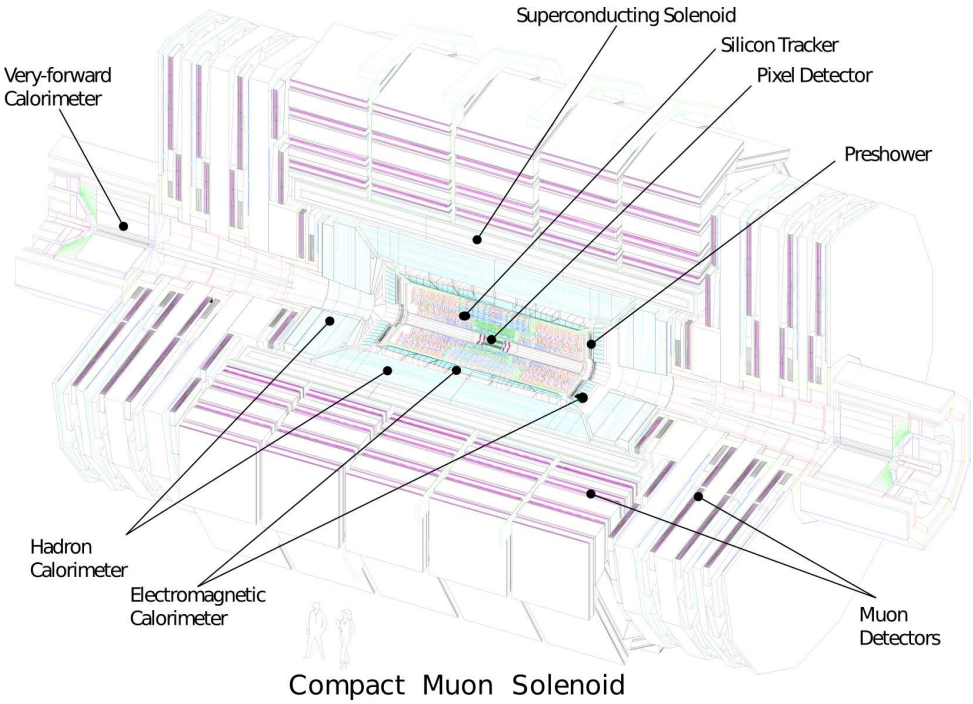

Figure 1: Cut through the CMS detector (from [1]).

The CMS detector is, next to ATLAS, one of the two main experiments at the LHC. Like most detectors it is composed of different layers serving the different purposes the

detector should meet.
The layout of the detector is shown in figure 2. In the following section the different parts of the detector are shortly discussed.

2.1 Inner tracking system

The inner tracking system of CMS is surrounding the interaction point in order to provide measurements of the trajectories of charged particles. It has a length of 5.8 m and a diameter of 2.5 m. It consists of a silicon pixel detector and a silicon strip detector. The solenoid provides a homogeneous 4 T field in the full volume of the tracker. The active silicon area of the tracker is about 200 m^2.
Right around the interaction point the pixel detector is assembled. It contributes tracking points in r, ρ and z. The dimensions of the silicon pixel are 100 x 150 μm. It consists of three barrel layers located 4.4, 7.3 and 10.2 cm from the interaction point and 2 end-cap disks located at $z = \pm 34.5$ and $z = \pm 46.5$ cm. Therefore, a detailed 3D tracking can be achieved.
The silicon strip tracker consists of an inner barrel with 4 layers and endcaps composed of 3 disks each and an outer barrel assembled out of 6 layers with endcaps consisting 9 layers each. The outer barrel extends up to a radius of 1.1 m with respect to the interaction point. Overall, the detector is composed of 15,148 strip modules.
Challenges in construction were finding radiation resistant materials to withstand the high particle flux and providing the desired granularity without introducing too much material for read out electronics into the system.

2.2 Electromagnetic calorimeter (ECal)

The ECal is assembled of 68,524 lead tungstate crystals. The high density of the crystals allows the calorimeter fast detection and radiation resistance. With 80% of the light being emitted within 25 nm, the scintillation decay time lies in the same order of magnitude as the bunch crossing of the LHC.

2.3 Hadronic calorimeter (HCal)

The hadronic calorimeter of the CMS detector is a sampling calorimeter, divided into two parts. The barrel calorimeter inside the solenoid is complemented by an outer calorimeter. The barrel calorimeter extends from $R = 1.77$ m to $R = 2.95$ m, while the outer calorimeter or tail catcher extends from the outer rim of the solenoid. A sampling calorimeter is assembled of alternating layers of absorbing material and scintillating material.

The calorimeter consists of 18 wedges in Φ direction. Each wedge is divided into 4 sectors. Therefore the barrel is divided into 72 sections in Φ direction. The η direction, describing the division in reference to the angle to the beam-pipe, there are 16 divisions to each side of the vertical direction. This results into an $\eta - \Phi$ segmentation of $(\Delta\eta, \Delta\Phi) = (0.087, 0.087)$.
In the CMS barrel HCal brass is used as the absorbing material, except for the first and last layer which are made out of stainless steel. The brass absorbers are made out of 70% Cu and 30% Zn. In Table 1 the layout of the different layers is shown.
The barrel calorimeter contains 17 layers of scintillating material as shown in Table 2. Layer 0 of the scintillators is located in front of the steel front plate and is therefore made out of a material with higher radiation hardness.
At the current state, the readout of the calorimeter does not involve a longitudinal segmentation. All scintillator signals are combined in one readout channel. For the CMS upgrade a longitudinal division into 4 readout channels is planned. Different readout designs have to be considered in order to optimize the gain of that upgrade.

Layer	**Material**	**Thickness**
front plate	steel	40 mm
1-8	brass	50.5 mm
9-14	brass	56.5 mm
back plate	steel	75 mm

Table 1: Absorber thickness in the barrel HCal

Layer	**Material**	**Thickness**
0	Bicron BC408	9 mm
1-15	Kuraray SCSN81	3.7 mm
16	Kuraray SCSN81	9 mm

Table 2: Scintillator thickness in the barrel HCal

2.4 Magnet

The superconducting solenoid magnet of CMS has been designed to reach a magnetic field of 4 T. The winding is composed of 4 layers. The solenoid has length of 12.5 m and an inner diameter of 6.3 m. The iron return yoke has a length of 13 m and an outer diameter of 14 m.

2.5 Muon system

The Muon system consists of several parts. 250 drift tubes (DTs) give two coordinates each. The DTs are arranged into three layers. The middle layer measures the coordinate parallel to the beam while the other two measure perpendicular.
Fig. 2.5 shows the principle of the measurement. Particles passing through the 4.2 cm wide drift tubes ionize the gas contained within. The electric field in between the wire (pointing into the page) and the tube walls accelerates the electrons, resulting in secondary ionizations and the hit is detected via the breakdown of the field. With the known drift speed of the electrons, the distance of the hit to the wire can be calculated. The other coordinate is given by the position on the wire where the hit is detected.

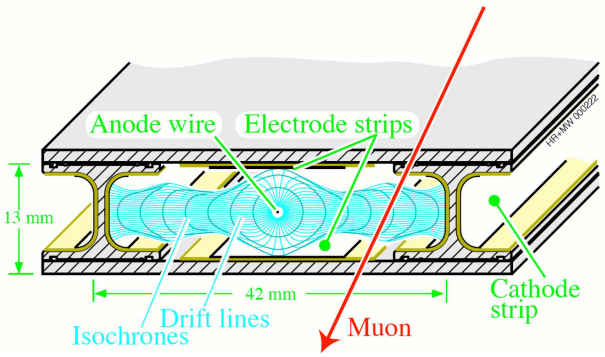

Figure 2: Schematic layout of the DTs (from [1]).

The endcap disks contain 540 cathode strip chambers (CSCs). These give 2 coordinates via a grid of copper strip cathodes with perpendicular wire anodes (cf. Fig. 2.5).

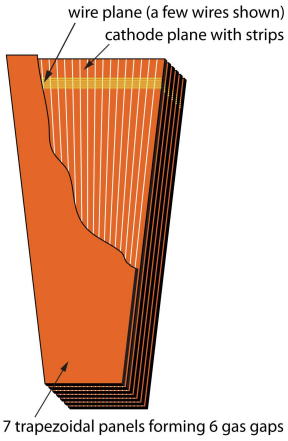

Figure 3: Schematic layout of the CSC (from [1]).

3 Simulating Data

One of the most important things in testing a new design for a detector is the simulation of Monte-Carlo events. Simulated data have the advantage, that the true values for the different properties are, unlike in the real experiment, accessible. Therefore, the detector can be evaluated on its precision and offset. The parameters gained from the simulated events can then be used for scaling and evaluating the real data.

3.1 Geant3 program

A Geant3 based program was used to simulate events.[2] Unlike the CMSSW software, it contains information about the energy deposition in the absorbers, needed to calculate the total energy deposition. Via the command "make hadron" a executable "hadron" is created on a 32-bit machine. In order to use the Gcalor shower algorithm, a second executable program "hadron_g" is created via "make hadron_g".
The executable program is run via a run file, "run_geant.sh", in which configurations can be made. In the run_geant.sh file the number of generated events, the beam energy, the type of particle and the position from which the particle is send to the target (i.e. onto the ECal, directly onto the HCal, etc.) can be defined. Also the random number seed can be changed in that file.
The shower algorithm used in the simulation can be adjusted in the hcal.txt_head file via the value of HADR. The TRIGGERS value defines the number of events contained in one file.
The configurations are stated in Table 3.

Particle type	**configuration**
Electron	3.
Muon	5.
Pion	8.
Proton	14.

Algorithm	**configuration**
Gheisha	3
Fluka	4
Micap	5
Gcalor	6

Starting point	**z-Value**
with ECal	-110
without ECal	-60
directly onto 1st HCal scintillator	-48.5

Table 3: List of configurations for simulation program

During the summer program the Monte-Carlo events as shown in Table 4 were created.

After simulating the events, they are stored in .root files, each containing 100 events. For further analysis the events should be stored in files containing all events of one configuration.
In order to achieve that, a root based program "skim" that combines all events into one file was used.[3] The program is also used to rename variables in a sensible way.

3.2 Shower algorithms

For over a decade it has been tried to simulate hadronic showers as realistically as possible. In this report 4 different shower algorithms, Fluka, Gheisha, Micap and Gcalor, have been used. As the comparison with the test beam data will show non of these perfectly simulate the process. They differ in various quantities.
In Fig. 3.3 the fractions of the energy that are deposited via electromagnetic, hadronic and invisible means are shown. One can easily see the different behavior of the algorithms. The most obvious difference is probably the significantly higher invisible fraction and the therefore lower electromagnetic fraction in the Gheisha algorithm.
In the e/π-ratio shown in Fig. 3.3 again the Gheisha algorithm behaves differently. The e/π-ratio is defined by

$$\frac{E^e_{\text{meas}}}{E^\pi_{\text{meas}}},$$

where E^e_{meas} is the measured energy when sending a electron beam directly onto the HCal and E^π_{meas} is the measured energy when sending a pion beam directly onto the HCal. In accordance to the graph it is therefore obvious, that Gheisha is the only shower algorithm in which the energy deposition for pions is bigger than that for electrons.

3.3 Comparison to test beam results

In a test beam experiment at CERN [4], the results shown in Fig. 3.3 have been measured by shooting an pion beam directly onto a part of the HCal. Comparing these results to the simulated events gives information about the quality of the Monte-Carlo data.
In Fig. 3.3 the energy distribution per layer from the Monte-Carlo events is shown. The different algorithms don't differ significantly in this property. However, the difference to the real data taken with the test beam is clearly visible. Therefore it can be concluded, that non of the shower algorithms perfectly describe reality.

Algorithm	Particle	Starting point	Energy [GeV]	Events
Fluka, Gheisha, Micap, Gcalor	e	direct HCal	5	50 000
Fluka, Gheisha, Micap, Gcalor	e	direct HCal	10	50 000
Fluka, Gheisha, Micap, Gcalor	e	direct HCal	20	50 000
Fluka, Gheisha, Micap, Gcalor	e	direct HCal	30	50 000
Fluka, Gheisha, Micap, Gcalor	e	direct HCal	50	50 000
Fluka, Gheisha, Micap, Gcalor	e	direct HCal	100	40 000
Fluka, Gheisha, Micap, Gcalor	e	direct HCal	150	40 000
Fluka, Gheisha, Micap, Gcalor	e	direct HCal	225	35 000
Fluka, Gheisha, Micap, Gcalor	e	direct HCal	300	35 000
Fluka, Gheisha, Micap, Gcalor	pi	direct HCal	5	50 000
Fluka, Gheisha, Micap, Gcalor	pi	direct HCal	10	50 000
Fluka, Gheisha, Micap, Gcalor	pi	direct HCal	20	50 000
Fluka, Gheisha, Micap, Gcalor	pi	direct HCal	30	50 000
Fluka, Gheisha, Micap, Gcalor	pi	direct HCal	50	50 000
Fluka, Gheisha, Micap, Gcalor	pi	direct HCal	100	40 000
Fluka, Gheisha, Micap, Gcalor	pi	direct HCal	150	40 000
Fluka, Gheisha, Micap, Gcalor	pi	direct HCal	225	35 000
Fluka, Gheisha, Micap, Gcalor	pi	direct HCal	300	35 000
Fluka, Gheisha	e	ECal	10	50 000
Fluka, Gheisha	e	ECal	20	50 000
Fluka, Gheisha	e	ECal	30	50 000
Fluka, Gheisha	e	ECal	50	50 000
Fluka, Gheisha	e	ECal	100	40 000
Fluka, Gheisha	e	ECal	300	35 000
Fluka, Gheisha, Micap, Gcalor	pi	ECal	5	50 000
Fluka, Gheisha, Micap, Gcalor	pi	ECal	10	50 000
Fluka, Gheisha, Micap, Gcalor	pi	ECal	20	50 000
Fluka, Gheisha, Micap, Gcalor	pi	ECal	30	50 000
Fluka, Gheisha, Micap, Gcalor	pi	ECal	50	50 000
Fluka, Gheisha, Micap, Gcalor	pi	ECal	100	40 000
Fluka, Gheisha, Micap, Gcalor	pi	ECal	150	35 000
Fluka, Gheisha, Micap, Gcalor	pi	ECal	225	30 000
Fluka, Gheisha, Micap, Gcalor	pi	ECal	300	30 000

Table 4: List of events generated

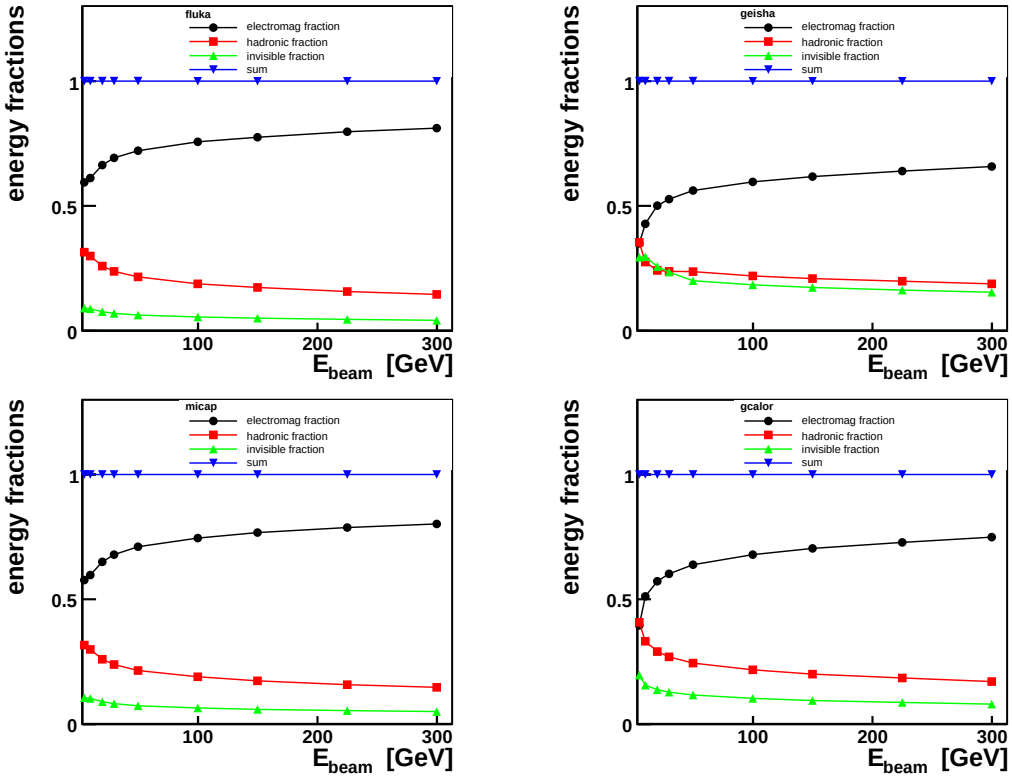

Figure 4: Energy fractions for the different shower algorithms.

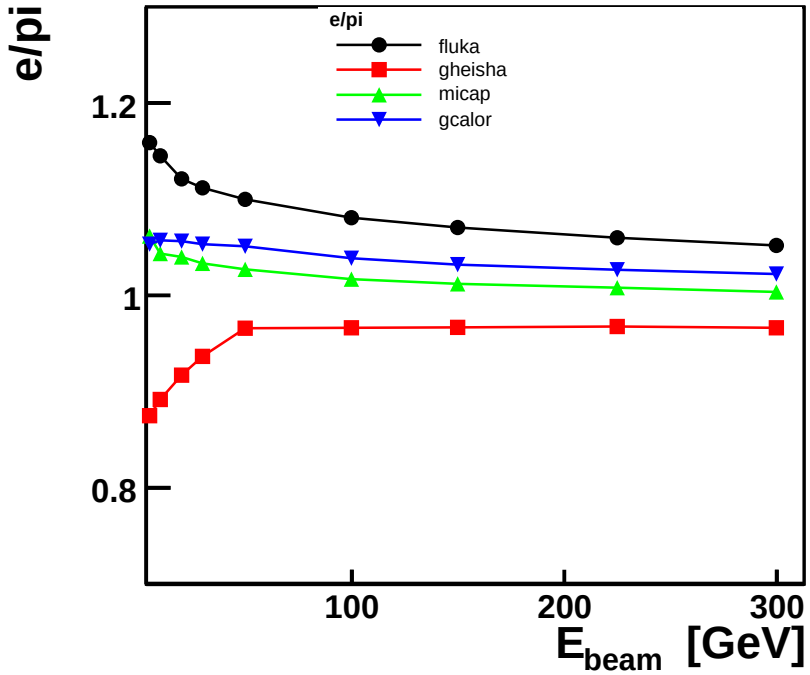

Figure 5: $\frac{e}{\pi}$- ratio.

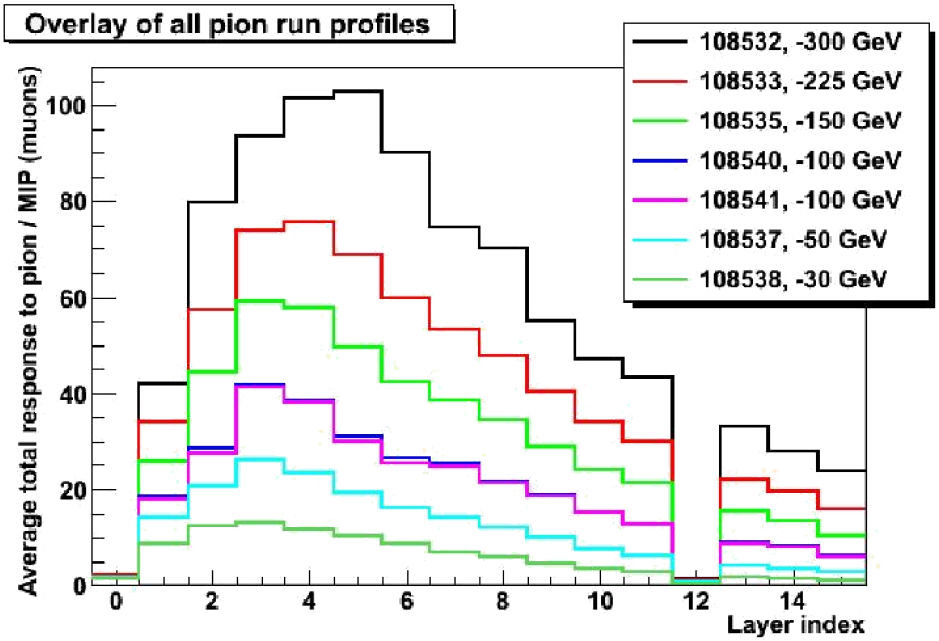

Figure 6: Energy per layer measured at the test beam. Layer 12 was damaged. [4]

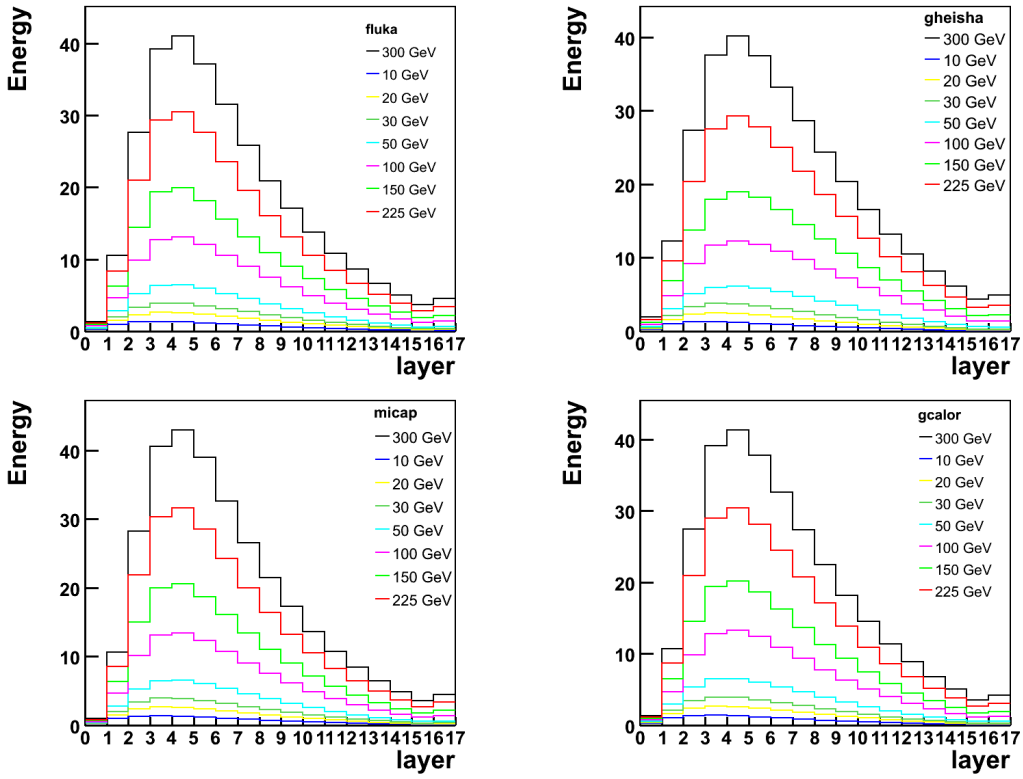

Figure 7: Energy per layer for the different shower algorithms.

4 Weighting

The relative energy deposition for electromagnetic and hadronic showers differs by a non-negligible amount. The different response influences the energy resolution and the linearity of the calorimeter. To truly identify the energy of the detected particles one therefore would need to differentiate between electromagnetic and hadronic energy deposition. This can be done via the varying energy density of the showers.
The energy density of hadronic showers is significantly smaller than that of electromagnetic showers. Therefore a possibility to correct for the different response would be to introduce a energy density dependent weighting factor. The weighting factors are calculated from

$$w_i(\rho_i, E^{beam}) = \langle \frac{E_i^{truth}}{E_i^{meas}} \rangle.$$

With sufficiently realistic Monte-Carlo simulations, weights for the different energy densities can be produced. A different approach would be to find a function fitting those weights in order to be able to weight every energy deposition exactly according to its energy density. The root based weighting program used in this work [5], uses Monte-Carlo events to generate weighting factors and weight the events with those. The goal is to realize an improvement in the linearity and the energy resolution. That is possible for energies up to 100 GeV. For higher energies the weighting does not improve the results.

4.1 Readout schemes and weighting results

For the planned CMS upgrade in 2014, the upgrade of the HCal involves a change of the readout-system of the scintillators. At the current state all scintillators are read out in one channel by a Hybrid Photo Detector (HPD) for the upgrade a change to Silicon Photo Multipliers (SiPM) is planned. Due to the smaller size a differentiated readout in several channels becomes possible. It is planned to introduce a 4 channel readout design. In the following a few readout designs are discussed. The numbering scheme starts with the lowest scintillator i.e. 1448 refers to a design where the 0th channel is read out separately followed by two blocks of 4 scintillators each (1-4 and 5-8) and a block of 8 in the end (9-16). The designs tested in this work are 1448, 2555, 15551 and 233333. Since 4 channels are planned in the upgrade, 1448 and 2555 are particularly interesting.
In Fig. 4.1- 4.1 the energy resolution for different designs using the different algorithms are shown. Focusing on the 4 channel designs, one can clearly see, that the 2555 design isn't gaining as much through the weighting as the 1448 design. This can be easily seen if a function

$$\left(\frac{\sigma(E)}{E}\right)^2 = \frac{a^2}{E} + c^2,$$

where $\frac{\sigma(E)}{E}$ is the energy resolution, a is the sampling term and c the constant term, is used to fit the points. The parameters and the relative improvement is shown in table 4.1. The same holds true for the linearity as shown in Fig. 4.1- 4.1.
In Fig. 4.1 and Fig. 4.1 a comparison between the different algorithms for the 1448 design is shown. Overall 1448 seems to be the better choice for improvement via the weighting.

Algorithm	**a [%]**	**c [%]**	**rel. Impr. [%]**	**a [%]**	**c [%]**	**rel. Impr. [%]**
	1448 readout design			**2555 readout design**		
Fluka	81.1	3.7		81.1	3.7	
weighted Fluka	66.3	7.5	18.3	68.4	4.9	15.7
Gheisha	114.9	0		114.9	0	
weighted Gheisha	96.7	4.4	15.8	96.6	0	15.9
Micap	83.7	0		83.7	0	
weighted Micap	65.9	6.4	21.3	69.6	2.9	16.9
Gcalor	95.3	0.8		95.3	0.8	
weighted Gcalor	74.0	7.2	22.3	77.4	4.3	18.8
	15551 readout design			**233333 readout design**		
Fluka	81.1	3.7		81.1	3.7	
weighted Fluka	64.5	7.9	20.5	69.1	5.4	14.9
Gheisha	114.9	0		114.9	0	
weighted Gheisha	94.0	5.1	18.2	97.4	0	15.2
Micap	83.7	0		83.7	0	
weighted Micap	65.0	6.6	22.3	70.3	3.1	16.0
Gcalor	95.3	0.8		95.3	0.8	
weighted Gcalor	72.5	7.6	24.0	79.0	4.3	17.1

Table 5: Improvement of the fit results for weighted events.

5 Conclusion

The weighting considerably improves the energy resolution and the linearity of the Monte-Carlo events. The 1448 readout design gives better possibilities for improvement than the 2555 system. In order to find the most promising readout design for the upgrade more investigations have to be done, e.g. with a modified CMSSW version that provides the absorber information as well.

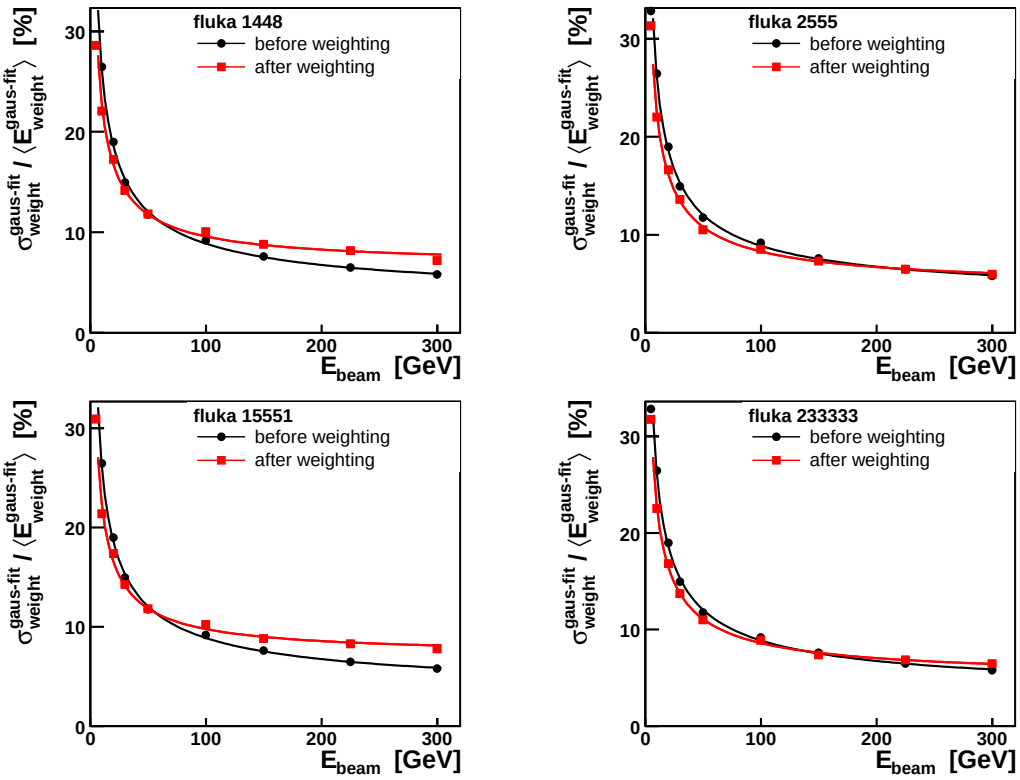

Figure 8: Energy resolutions for the different readout-schemes for the Fluka algorithm.

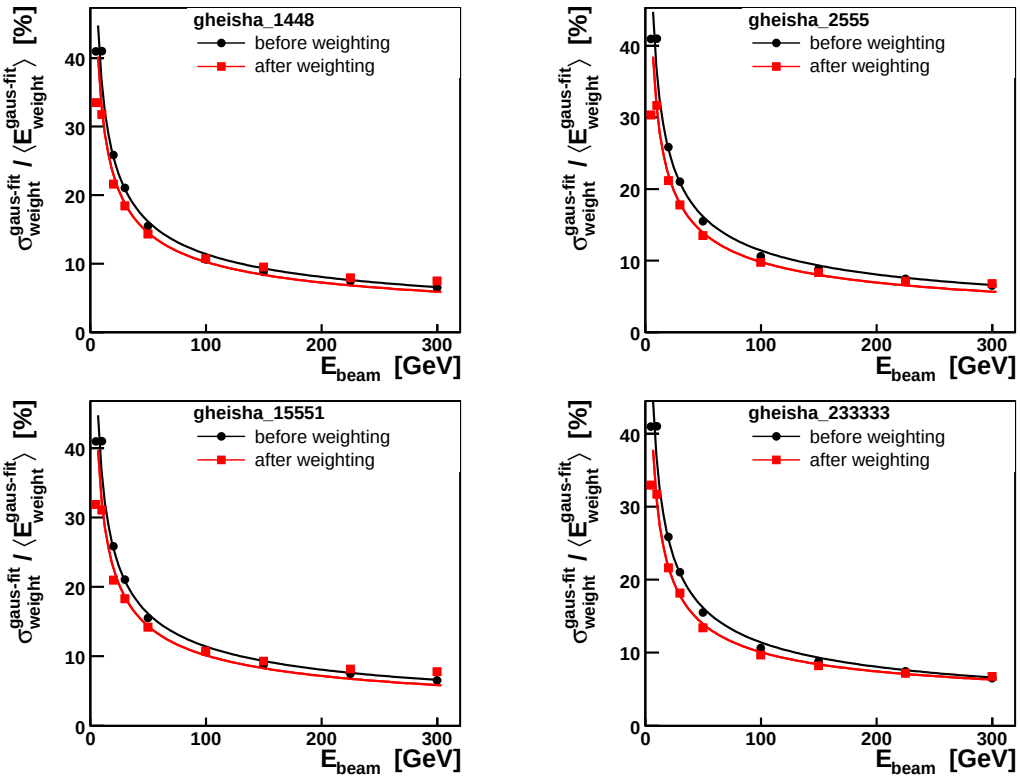

Figure 9: Energy resolutions for the different readout-schemes for the Gheisha algorithm.

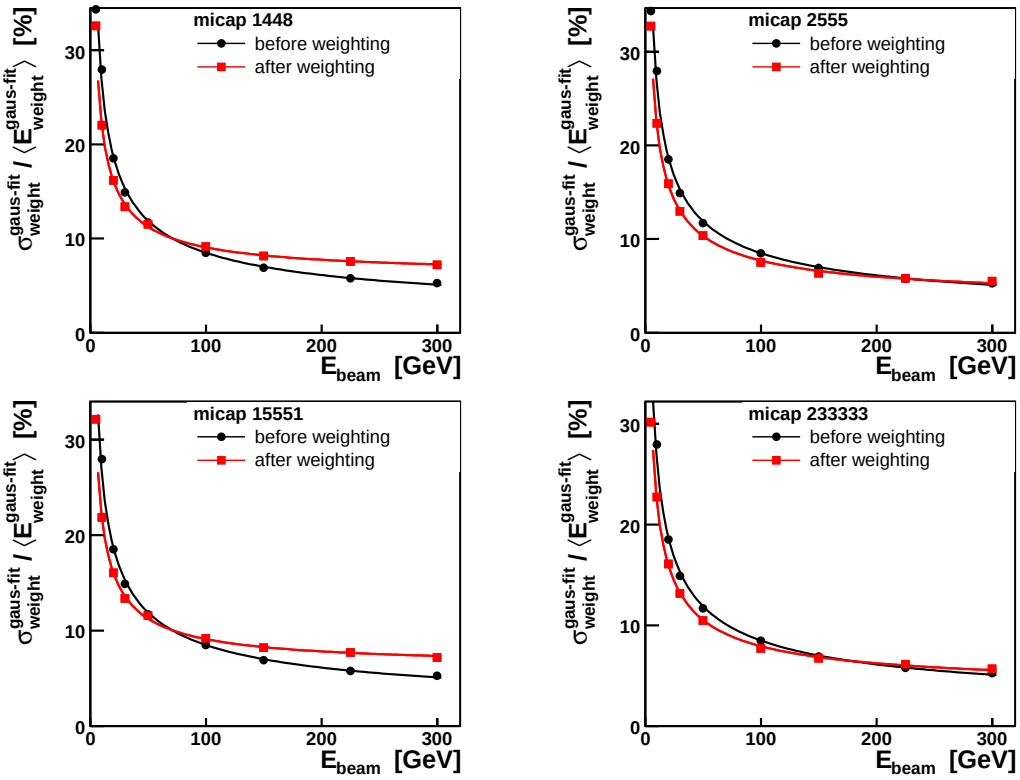

Figure 10: Energy resolutions for the different readout-schemes for the Micap algorithm.

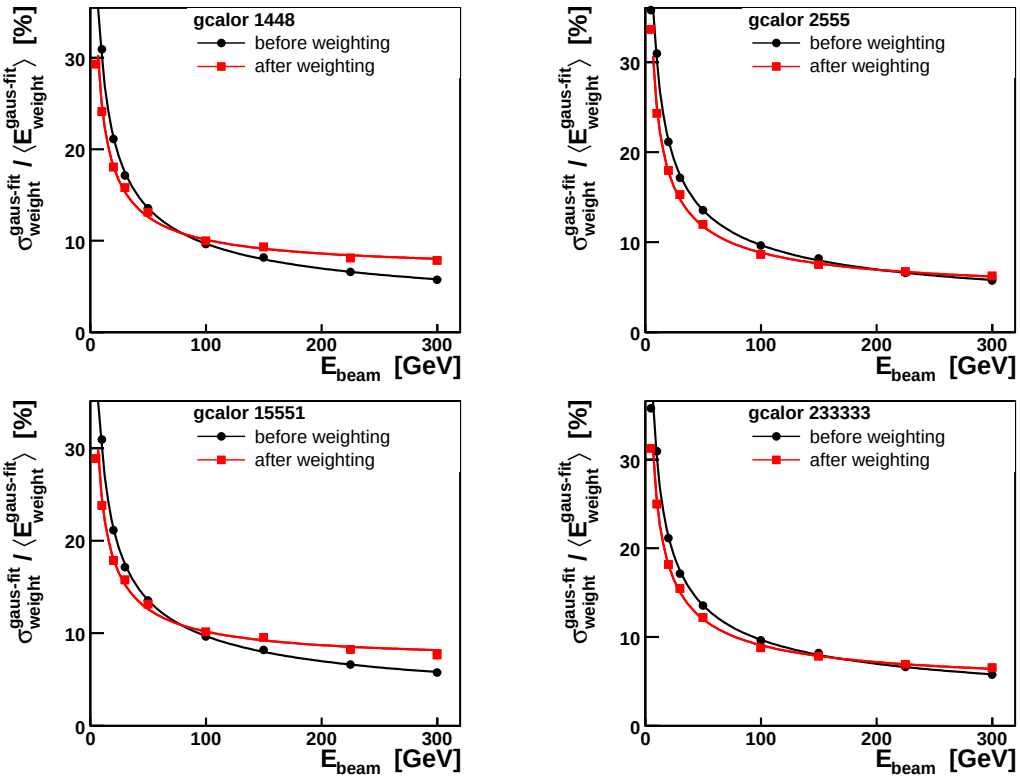

Figure 11: Energy resolutions for the different readout-schemes for the Gcalor algorithm.

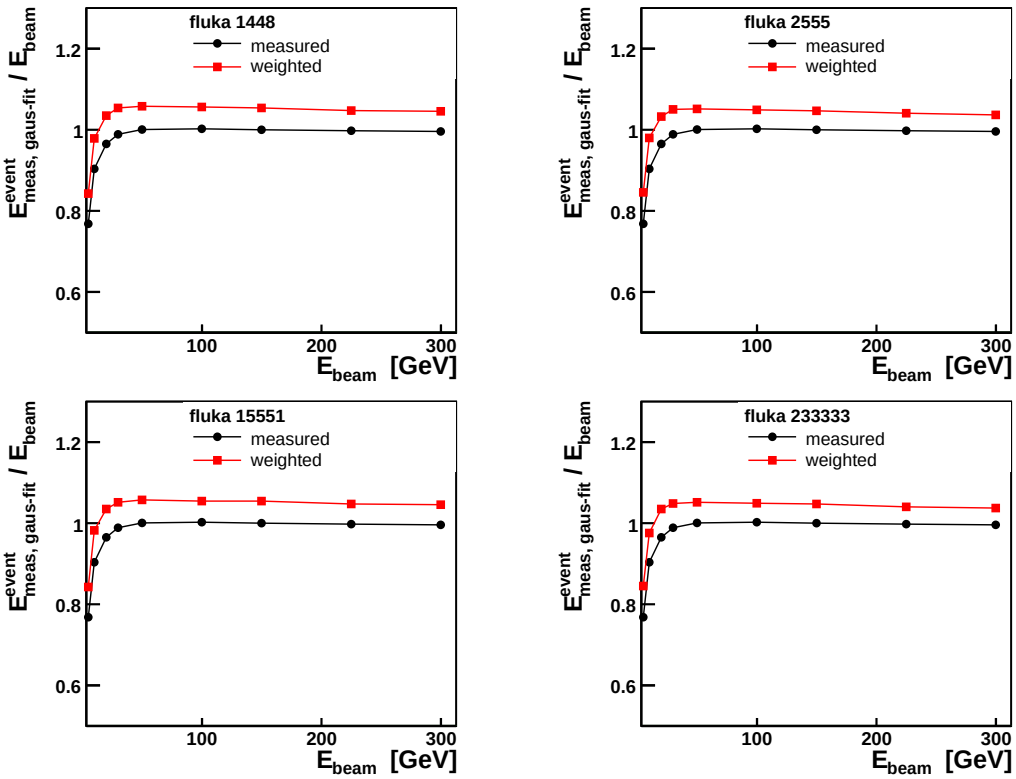

Figure 12: Linearity for the different readout-schemes for the Fluka algorithm.

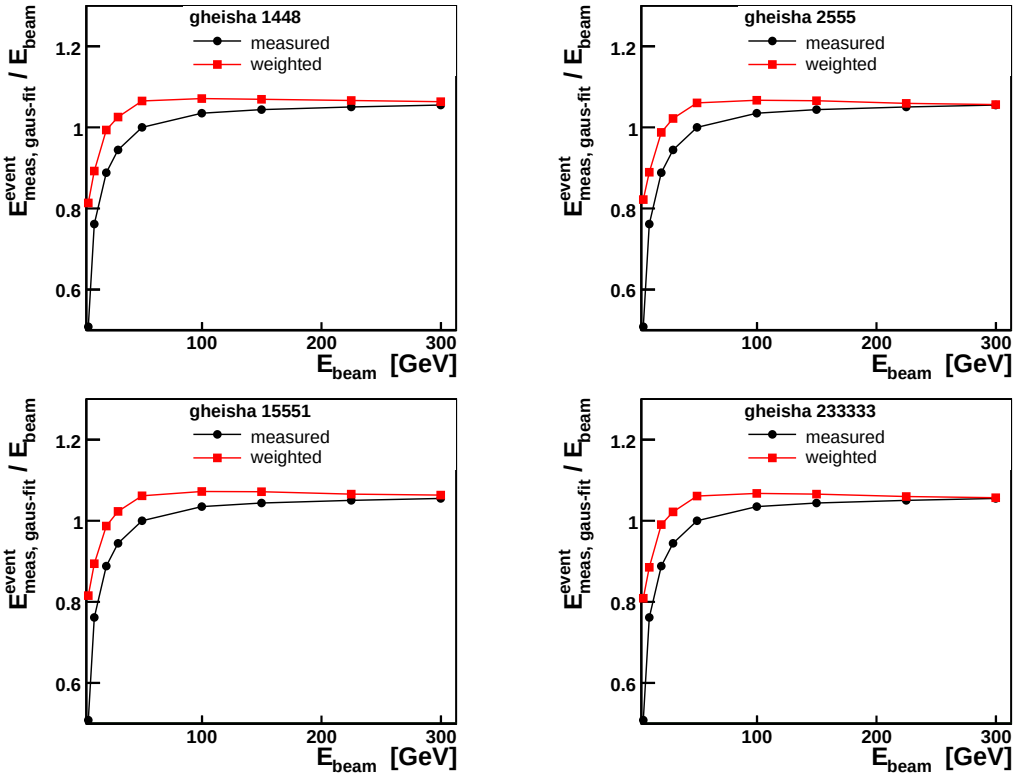

Figure 13: Linearity for the different readout-schemes for the Gheisha algorithm.

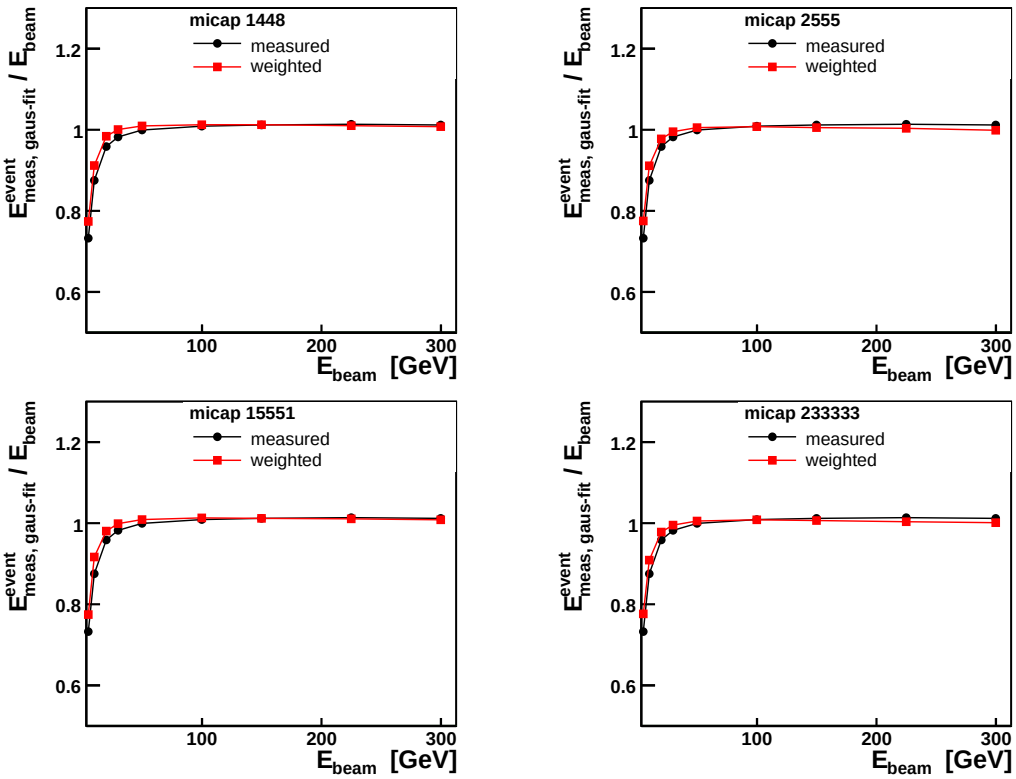

Figure 14: Linearity for the different readout-schemes for the Micap algorithm.

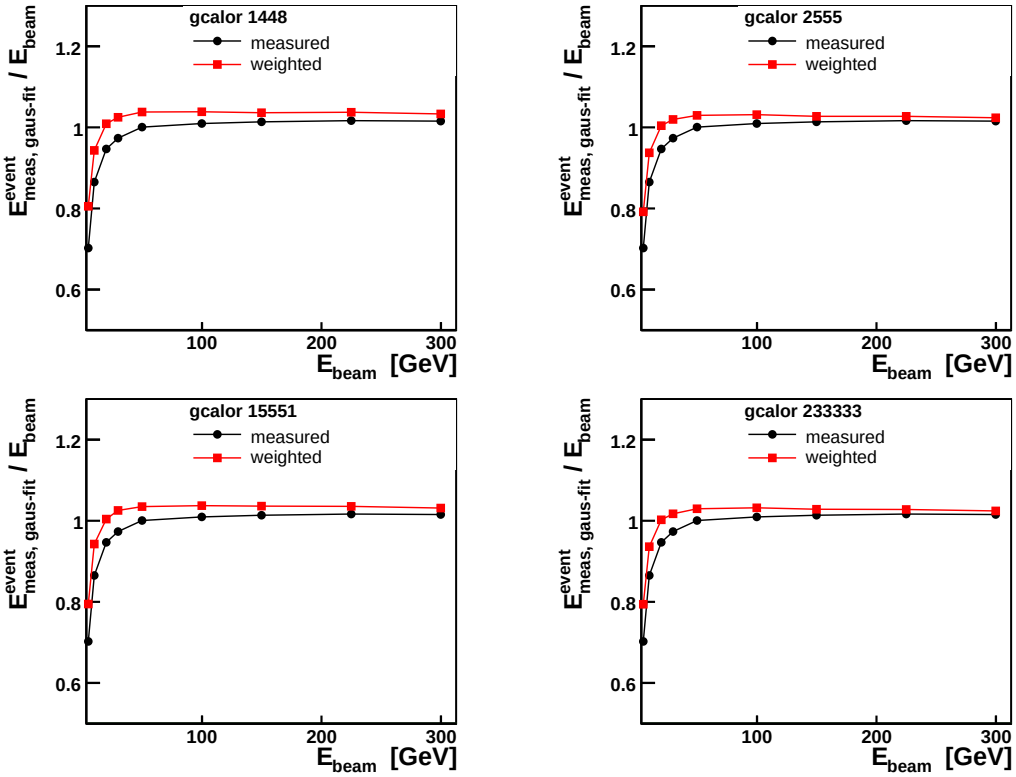

Figure 15: Linearity for the different readout-schemes for the Gcalor algorithm.

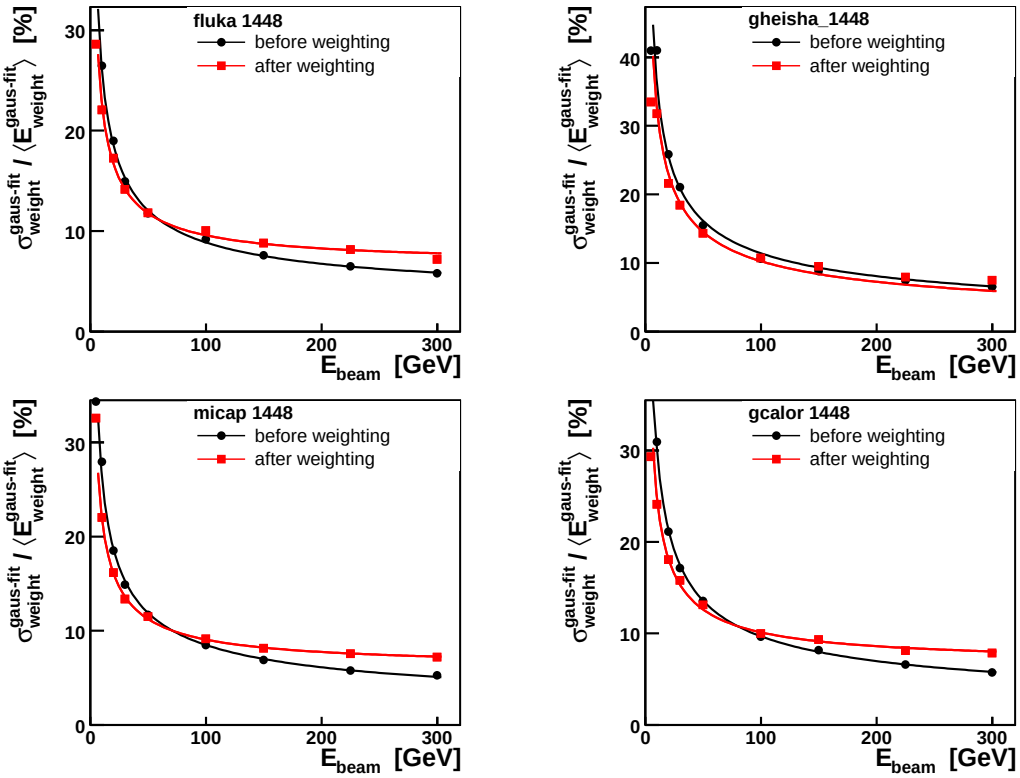

Figure 16: Energy resolution for the different shower algorithms for the 1448 readout design.

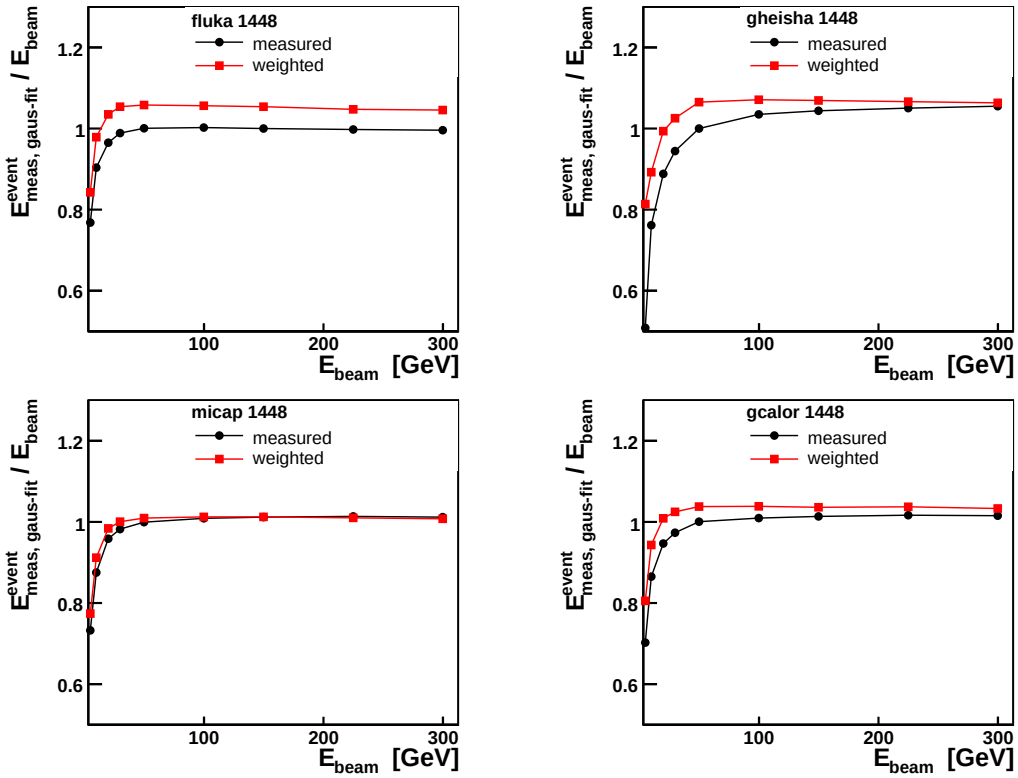

Figure 17: Linearity for the different shower algorithms for the 1448 readout design.

References

[1] The CMS experiment at the CERN LHC *CMS Collaboration*

[2] Geant3 based simulation program *Vladimir Andreev*

[3] Root based skim program *Matthias Stein*

[4] TB '09 Mulitlayer Readout Report *Chen, Fitzpatrick, Laird, et al.*

[5] Root based weighting program *Matthias Stein*